Volume 1 | Number 1 | Jan 2013 | Pages 1–100

Nanoscale

www.rsc.org/nanoscale

ROYAL SOCIETY
OF CHEMISTRY

This is an *Accepted Manuscript*, which has been through the
Royal Society of Chemistry peer review process and has been
accepted for publication.

Accepted Manuscripts are published online shortly after
acceptance, before technical editing, formatting and proof reading.
Using this free service, authors can make their results available
to the community, in citable form, before we publish the edited
article. We will replace this *Accepted Manuscript* with the edited
and formatted *Advance Article* as soon as it is available.

You can find more information about *Accepted Manuscripts* in the
Information for Authors.

Please note that technical editing may introduce minor changes
to the text and/or graphics, which may alter content. The journal's
standard **Terms & Conditions** and the **Ethical guidelines** still
apply. In no event shall the Royal Society of Chemistry be held
responsible for any errors or omissions in this *Accepted Manuscript*
or any consequences arising from the use of any information it
contains.

ROYAL SOCIETY
OF CHEMISTRY

www.rsc.org/nanoscale

Nanoscale

COMMUNICATION

Compact chelator-free Ni-integrated CuS nanoparticles with tunable near-infrared absorption and enhanced relaxivity for in vivo dual-modal photoacoustic/MR imaging

Duyang Gao,[a†, c] Pengfei Zhang,[a†, d] Chengbo Liu,[b†] Chi Chen,[a] Guanhui Gao,[a] Yayun Wu,[a] Zonghai Sheng,[a] Liang Song[b] and Lintao Cai [a] *

A chelator-free doping method is developed for constructing Ni-integrated CuS nanostructure as a novel PA/MRI contrast agent. It exhibits tunable near-infrared absorption spectral. Moreover, the hybrid nanostructure has demonstrated dramatic enhanced T1 relaxivity compared with Ni ions. Due to these unique properties, the chelator-free nanoparticles have been successfully applied for in vivo PA/MRI dual-modal imaging.

Multimodal imaging has attracted intensive attention for offering versatile imaging tools for biomedical applications. [1] Integrating the complementary merits of different imaging modalities is an effective approach to extract accurate and reliable biomedical information, thus improving the efficacy and sensitivity of clinical imaging diagnostics. [2] Magnetic resonance imaging (MRI) is considered a powerful imaging modality and widely used in human medicine for the last two decades. [3] As one of the new generation non-invasive hybrid imaging techniques, photoacoustic (PA) imaging, a synergistic combination of optical and ultrasound imaging technologies, provides unprecedented advantages of the high contrast of optical imaging as well as the high resolution of acoustic imaging at centimeter penetration depth. [4] Therefore, new imaging technique that integrated MRI with PA, which not only depict subsurface tissue structures, but also offer higher resolution and deeper tissue penetration, will lead to better diagnosis of many diseases. [5]

Nanotechnology provides a flexible platform for the development of effective multimodal contrast agents by integrating components that provide image contrast based on different properties, including optical and magnetic properties. [6] For example, metallic nanoparticles (NPs), especially gold nanorods/nanoshells/nanocages, with near-infrared (NIR) optical absorption, have been constructed as PA agents because of their tunable localized surface plasmon resonance (LSPR). [7] Very recently, copper-based NPs have also been prepared with NIR absorption, [8] which proved to be better PA agents than gold nanostructures because of their smaller size and broader NIR absorbance. [9] Besides, NPs composed of transition metal are often involved in MRI, such as Fe_3O_4, $NaGdF_4$, Co_9Se_8, and so on. [10] To integrate these functionalities together, two most popular processes have been established as following: (i) loading or coupling, such as $Fe_3O_4@Au$; (ii) growing self-assembly, such as $Au-Cu_9S_5$, $Fe_3O_4@CuS$. Both of them have been proved to be effective methods to construct multifunctional NPs. [11] However, there are intrinsic limitations for these methods. The former method usually needs chelator which will influence the surface properties of the NPs and reduce the capability of conjugating other targeting or therapeutic agents. [1b, 12] The latter method involves complicated and multi-step synthetic processes which would lead poor repeatability. Therefore, chelator-free and simple synthesis of multifunctional NPs and integration of multiple design components remain challenging. Doping, which can integrate functional ions into nanostructure by one-step and meets all the demands, is a promising method to design multifunctional NPs. It has also been used for constructing various kinds of multimodal contrast agents, such as MRI/UCL, PET/FL, MRI/FL, PET/CT, and so on. [1a, 1c, 1d, 13] However, little efforts have been made on establishing PA/MRI imaging contrast agents by this method.

Herein, we developed a doping method for constructing Ni-integrated CuS nanostructure as a new PA/MRI contrast agent. The chelator-free Ni-integrated CuS NPs have been synthesized based on high temperature reaction in non-polar solvents by one-step (**Scheme 1**). The resulted CuS-based dual-modal contrasts agent mainly possess the following

a. Guangdong Key Laboratory of Nanomedicine, CAS Key Laboratory for Health Informatics, Shenzhen Bioactive Materials Engineering Lab for Medicine, Institute of Biomedicine and Biotechnology, Shenzhen Institutes of Advanced Technology, Chinese Academy of Sciences, Shenzhen, 518055, P. R. China. E-mail: lt.cai@siat.ac.cn
b. Research Lab for Biomedical Optics and Molecular Imaging, Shenzhen Key Lab for Molecular Imaging, Institute of Biomedical and Health Engineering, Shenzhen Institutes of Advanced Technology, Chinese Academy of Sciences, Shenzhen 518055, P. R. China
c. Bioimaging Core, Faculty of Health Sciences, University of Macau, Macao, China
d. Division of Biomedical Engineering, The Hong Kong University of Science and Technology, Clear Water Bay, Kowloon, China
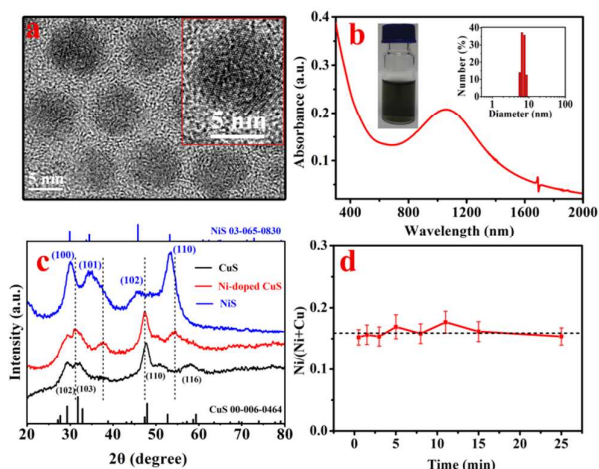† All authors contributed equally.
Electronic Supplementary Information (ESI) available: details of the experimental procedure and supplementary Fig.S1 to S5 See DOI: 10.1039/x0xx00000x
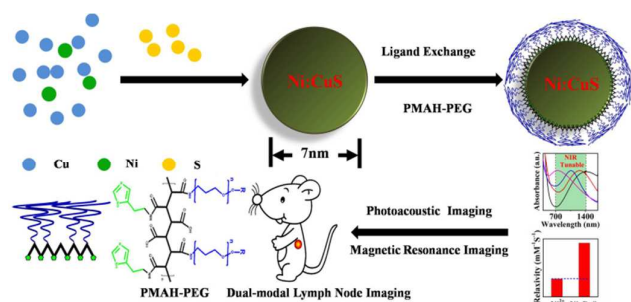
Scheme 1. Schematic illustration of chelator-free Ni-integrated CuS NPs for in vivo dual-modal lymph node imaging.

Fig. 1. (a) High-resolution transmission electron micrograph of Ni-doped CuS NPs with average size of about 7 nm; (b) absorption spectrum photograph under light (insert left) and diameter measured by DLS (insert right) of the doped NPs dispersed in chloroform; (c) X-ray power diffraction data of the as-prepared CuS, NiS and Ni-doped CuS; (d) A plot of particle composition (measured by inductively coupled plasma optimal emission spectrometry) versus time of Ni-doped CuS NPs.

advantages: i) small size with highly crystalline; (ii) uniform distribution and well reproducible preparation. The chelator-free Ni-doped CuS NPs exhibit tunable absorption spectral covers NIR-I (700 nm-950 nm) and NIR-II (950 nm - 1300 nm) "biological widow", where absorption and scatting by tissues, blood and water are minimized. [11b] The NIR absorbance property is responsible for PA imaging by 1064 nm laser irradiation. More importantly, the hybrid nanostructures also have demonstrated dramatic enhanced T1 relaxivity in comparison to Ni ions, which is an essential evaluating parameter of MRI contrast agents. To the best of our knowledge, enhanced T1 relaxivity by doping Ni ions into CuS NPs has not reported before. Furthermore, the as-prepared NPs are easily coated with polymers (Fig. S1) rich in imidazole groups along the backbone for further biological applications. Due to the tunable NIR absorption and enhanced T1 relaxivity, the chelator-free Ni-doped CuS NPs have been successfully demonstrated in the potential applications for in vivo lymph node PA/MRI dual-modal imaging. Consequently, it provides a promising and robust method to construct PA/MRI dual-modal NPs, which can also involve other interesting metal ions to design multifunction nanostructures.

Solution-based high temperature reactions were carried out to prepare Ni-integrated CuS NPs. Transmission electron microscopy (TEM) images showed that the Ni-doped CuS NPs had good monodispersity with an overall diameter of about 7 nm (Fig. S2), which were further confirmed by high-resolution TEM (HRTEM) (Fig. 1a) and dynamic light scattering (DLS) (insert in Fig. 1b). As displayed in Fig. 1a, the HRTEM images of Ni-doped CuS NPs revealed that a uniform spherical shape was obtained with well-resolved lattice fringes, demonstrating the highly crystalline nature of the as-prepared NPs. The absorption spectrum of the NPs was displayed in Fig. 1b. Interestingly, the absorbance of the Ni-doped CuS NPs was above zero over the range of wavelength probed. A strong absorbance peak centered at about 1060 nm was also clearly observed in the spectrum. The appearance of this characterize absorption can be attribute to scatting, LSPR or other reasons. An obvious character of LSPR was the sensitivity of absorption band to solvents of different refractive index. We compared the NIR absorption spectra of the Ni-doped CuS NPs in four different solvents: hexane, toluene, chloroform and carbon

disulfide with refractive index of 1.375, 1.496, 1.448 and 1.629, respectively. The NIR absorbance continuously red-shifted with increasing refractive index of the solvent in which the Ni-doped CuS NPs were dispersed, as expected for LSPR absorbance (Fig. S3). Given these data, we confidently attributed the NIR absorption band to LSPR, which was also consistent with the Cu-based nanocrystals previously reported. [14] The photograph under light and DLS measurement were used to characterize the NPs dispersed in chloroform. As displayed in Fig. 1b insert, the solution with concentration ten times of sample used for the absorption measurement (Fig. 1b) was dark-brown. There was no precipitation can be seen in the solution. It was also confirmed by the DLS experiment since there was only one peak in Fig. 1b insert. The crystalline structure of the as-prepared NPs was measured by powder X-ray diffraction (XRD). As displayed in Fig. 1c, the crystal structure of CuS and NiS can be assigned as a typical hexagonal structure with the existence of strong characteristic (102), (103), (110), (116) and (100), (101), (102), (110) peaks, respectively. It was noted that the peaks of doped NPs were intermediate between CuS and NiS. The peak shifting of the NPs also indicated that there was no phase separation or isolated nucleation of CuS or NiS in the doped NPs. Batches of NPs with periodic removal of aliquots of the growing NPs were washed and analyzed by inductively coupled plasma optimal emission spectrometry (ICP-OES) to confirm the composition of the doped NPs. As demonstrated in Fig. 1d, the composition remained nearly constant during growth periods. This set of elemental data provided strong evidence that the ternary NPs have a homogeneous alloy structure from start to the end of
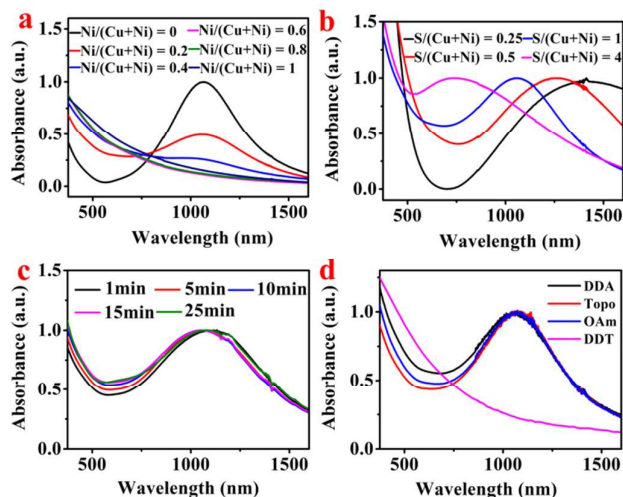
Fig. 2. UV-VIS-NIR absorption spectra of different Ni content (a), S content (b), reaction time (c) and ligands (d) of the as-prepared NPs dissolved in CHCl$_3$

particle growth. Energy dispersive spectroscopy (EDS) was also conducted to confirm the element of the NPs (Fig.S4).

A collection of plasmonic absorbance from Ni-doped NPs prepared under a variety of modified conditions was shown in Fig. 2. The absorbance intensity of the NPs was continuously reduced with increased Ni content (Fig. 2a). The LSPR absorbance peak was blue-shifted from 1400 nm to 740 nm with increasing addition of S element (Fig. 2b). The blue-shift mainly ascribed to the presence of excess S element which possessed weak oxidability. As the oxidation proceeded, an increasing number of vacancies were produced. The resulting increase in free carrier concentration leaded to a blue shift of the absorbance. [15] Thus, we concluded that Cu content played an important role in determining the LSPR absorbance intensity while S element mainly effected the LSPR peak position. The effect on LSPR absorbance of reaction time was also studied. As shown in Fig. 2c, despite the variation, all of the Ni-doped NPs were found to exhibit qualitatively similar absorbance spectra with an intense NIR absorption peak. Ni-doped CuS NPs with different ligands including DDA, Topo, OAm and DDT were prepared under the same conditions. The LSPR absorbance were also displayed in Fig. 2d. Interestingly, all the NPs had nearly same absorption spectra except the DDT modified NPs. The characterized absorption peak had been disappeared with the addition of DDT. HRTEM images of the DDT modified NPs had been displayed in Fig. S5. An obvious change had been observed on the shape of the Ni-doped CuS NPs. Rod-shape of the DDT modified monodisperse NPs had been appeared instead of spherical as other ligands. The phenomenon was also consistent with previous report. [16]

For further biological applications, ligands exchange was carried out to make the hydrophobic Ni-doped CuS NPs water-dispersible. The as-prepared NPs with 20% doping content were chosen to implement the following experiments for their

adequate absorption which was not only in the range of near infrared region, but also can be matched with the laser source of the home-built PA equipment. Schematic representation of the Ni-doped CuS NPs with images of the organic and aqueous dispersions was displayed in Fig. 3a. It indicated that ligands exchange of Ni-doped CuS NPs (capped with the native OAm) can be carried out using a pegylated multidentate polymer with imidazole pendant groups (PMAH-PEG, Fig.S1), which was reported by our group previously. [17] Upon ligands exchange with PMAH-PEG, the hydrophilic NPs were dispersed well (Fig.S6). Moreover, there was no precipitation of the water-soluble NPs after about fifteen days as shown in Fig. 3b. Additionally, the absorption spectra, hydrodynamic size and zeta potential of the PMAH-PEG-capped Ni-doped CuS NPs were tested. As shown in Fig. 3c, hydrophilic NPs exhibited identical absorption spectral profiles compared to those of initial hydrophobic NPs dispersions in chloroform. The hydrodynamic size of the NPs was also measured by DLS. As shown in Fig. 3d, the diameter of PMAH-PEG-capped NPs was about 26 nm after ligands exchange which was larger than OAm-capped NPs dispersed in chloroform as mentioned before. This was because the NPs were charged in water, thus creating an electrical double layer on the NPs surface which increased the colloidal hydrodynamic diameter. Besides, there was only one peak in Fig. 3d, which also illustrated that these Ni-doped CuS NPs were transferred into aqueous solution without aggregation. In addition, zeta potential of the PMAH-PEG-capped NPs was also measured to be a negative potential nearly -26 mV as displayed in Fig. 3e. Stability of the NPs were critical for their further biological applications, such as in vitro and in vivo imaging. Therefore, the stability of the resulted water-dispersible PMAH-PEG-capped NPs was characterized. As shown insert of Fig. 3c, Fig. 3d and Fig. 3e, the absorption, diameter and zeta potential of the water-soluble NPs had nearly no change under ambient condition for about half a month, which indicated that the PMAH-PEG-capped NPs exhibited excellent storage stability.

In vitro PA imaging and MRI experiments were carried out in order to investigate the potential capability of PMAH-PEG-capped NPs for dual-modal imaging. Fig. 3f showed the maximum amplitude projection (MAP) PA image of a clear agar phantom filled with PMAH-PEG-capped NPs of four different concentrations (0.125 mg mL^{-1}, 0.25 mg mL^{-1}, 0.5 mg mL^{-1}, 1.0 mg mL^{-1}). Moreover, the PA signals generated by the water-soluble NPs were observed to be linearly dependent on the concentration ($R^2 = 0.9904$). The linear range was from 0.125 mg mL^{-1} to 1 mg mL^{-1} (Fig. 3f). Additionally, there was no Ni ions released from the NPs after in vitro PA imaging (Table S1). MRI capabilities of the NPs dissolved in water were also measured. T1-weighted images in Fig. S7 clearly exhibited the enhanced MR signal intensities. The R1 (1/T1) relaxivity at different concentrations (0, 0.0113, 0.0337, 0.101, 0.304, 0.912 mM) of Ni^{2+} containing NPs or single Ni^{2+} were detected, and plotted against the concentrations. The R1 was determined from the slope of the linear plot of 1/T1 versus Ni^{2+} concentration (Fig. 3g). From the plot, we obtained the specific relaxivity of PMAH-PEG-capped

Nanoscale

COMMUNICATION
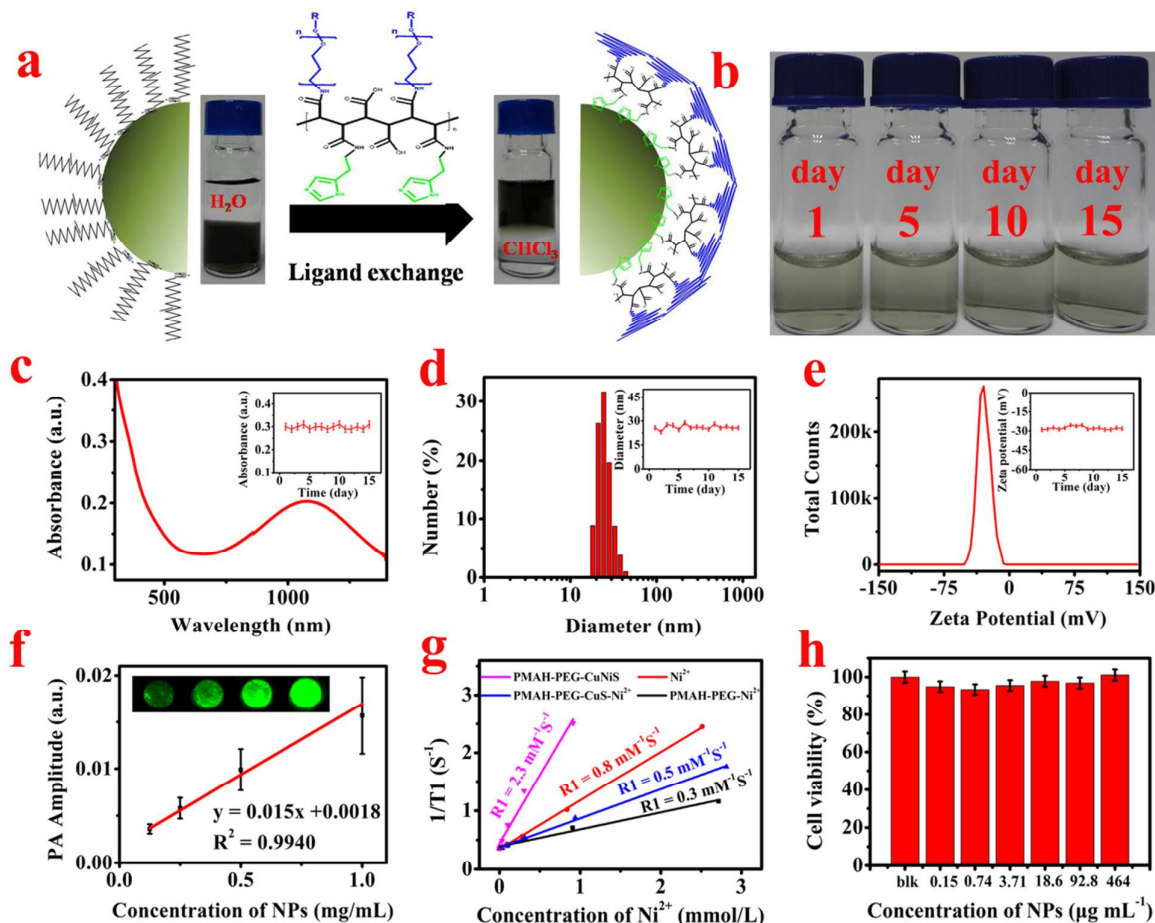
Fig. 3. (a) Schematic representation of the Ni-doped CuS NPs with images of the organic and aqueous dispersions; (b) Stability test of the water-soluble Ni-doped CuS NPs dispersed in PBS at pH 7.4; (c) UV-VIS-NIR absorption spectra, (d) diameters measured by dynamic light scatting, and (e) zeta potential of Ni-doped CuS NPs after ligands exchange with PMAH-PEG and the insert of each displayed the stability of the NPs; (f) PA images of PMAH-PEG-capped NPs with different concentrations and the linear relationship between PA signal intensity and the different concentrations of NPs; (g) Plots of $1/T1$ (s^{-1}) as a function of Ni^{2+} concentration for the correlated materials. The slope indicated the specific relaxivity (2.3 $mM^{-1}S^{-1}$ for PMAH-PEG-CuNiS, 0.8 $mM^{-1}S^{-1}$ for Ni^{2+}, 0.5 $mM^{-1}S^{-1}$ for PMAH-PEG-CuS-Ni^{2+}, 0.3 $mM^{-1}S^{-1}$ for PMAH-PEG-Ni^{2+}); (h) Cell viability of MCF-7 cells recorded after being incubated with water-soluble Ni-doped CuS NPs.

Ni-doped CuS was 2.3 $mM^{-1}S^{-1}$. Furthermore, the relaxivity of Ni^{2+}, PMAH-PEG-Ni^{2+} and Ni^{2+} adsorbed PMAH-PEG-CuS were also measured. The slopes of them were smaller than that of water-soluble Ni-doped CuS NPs. It indicated PMAH-PEG-capped Ni-doped CuS NPs had highest relaxivity compared to the others. Amazingly, the relaxivity of Ni-doped CuS NPs was up to 8 times higher than that of PMAH-PEG-Ni^{2+}. The enhancement of the relaxivity was probably attributed to the geometrical confinement of the nanostructure, which influenced the magnetic behavior of the Ni^{2+} ions. The phenomenon was consistent with the paramagnetic Gd^{3+} ions as previously reported.[18] Importantly, this relaxivity value appeared to be comparable to that of commercial MRI contrast agents such as Teslascan (1.6$mM^{-1}S^{-1}$), Feridex (2.3 $mM^{-1}S^{-1}$), Prohance (2.8 $mM^{-1}S^{-1}$) and Dotarem (2.8 $mM^{-1}S^{-1}$). However, it is still lower than that of some commercial
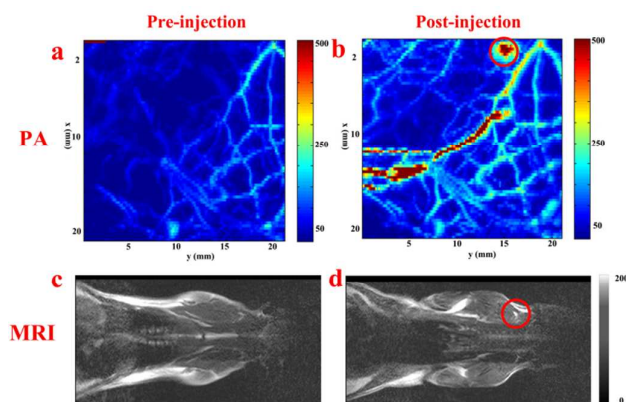
Fig. 4. In vivo PA imaging of mouse before (a) and after (b) injected with 0.05 mL (0.4 mg mL^{-1}) PMAH-PEG-capped Ni-doped CuS NPs; T1 weighted MRI of the mouse before (c) and after (d) injection of the dual-modal nanoprobe. Red circle indicated the lymph node.

contrast agents such as Magnevist (3.2 mM^{-1}S^{-1}), Gadovist (3.2 mM^{-1}S^{-1}) and Omniscan (3.3 mM^{-1}S^{-1}), as reported by Rohrer *et al*. [19]. In addition, the relaxivity measured is per nickle ion and would be much higher per NPs. This result illustrated that PMAH-PEG-capped Ni-doped CuS NPs would have significant potential applications as a contrast agent in MRI. In addition, the PMAH-PEG-capped Ni-doped CuS NPs showed no cytotoxicity tested at 0.46 mg mL^{-1} NPs highest concentration as shown in Fig. 3h and Fig. S8.

The lymphatic system is a major pathway for the spread of cancer. Therefore, it is of great importance to image lymph node for diagnosis of the metastatic stage of cancer. [20] In order to determine whether PMAH-PEG-capped Ni-doped CuS NPs could be used for *in vivo* PA and MR imaging, the water-soluble NPs with a concentration of 0.4 mg mL^{-1} was injected subcutaneously into the distal part of the right anterior paw of healthy mice for regional lymph node mapping.

The lymph node in the right axillary location was monitored by our home-built noninvasive reflection-mode PAT system. [1f] As the PMAH-PEG-capped Ni-doped CuS NPs traveled through the lymphatic vessels and accumulated to the lymph node, a robust PA signal within the lymph node was captured up to 30 minutes post-injection. As shown in Fig. 4a, the pre-injection image clearly showed the axillary blood vessel (BV) networks, but not the lymph node. After injection, the PA signal in lymph node was enhanced dramatically. The corresponding PA B-scan images obtained from Fig. 4a and Fig. 4b had been displayed in Fig. S9, respectively, providing depth (i.e., z direction) information of blood vessels and the lymph node. The MRI experiment was performed using a clinical 3 Tesla horizontal bore magnet (SIEMENS, VERIO). There was nearly no signal in the lymph node before injection of the NPs (Fig. 4c), however, as shown in Fig. 4d, the lymph node was observable after injection, which was in accordance with PA imaging experiment result. It indicated PMAH-PEG-capped Ni-doped

CuS NPs can be used as PA/MRI dual-modal nanoprobes for biomedical imaging.

Conclusions

In conclusion, we reported a facile and reliable approach for the synthesis of small homogeneous alloyed chelator-free Ni-integrated CuS NPs with strong NIR absorption, which was definitely tuned between 740 nm and 1400 nm. The peak position of the LSPR absorption exhibited S-dependent, while the doped Ni^{2+} ions had a significant impact on the peak intensity. Pegylated multidentate polymers were introduced to make biocompatible hydrophilic Ni-doped CuS NPs for potential biological imaging. The water-dispersible NPs have shown compact sizes and excellent stability under ambient condition for nearly two weeks. The NPs were proved to be good contrast agents not only for PA imaging due to their NIR LSPR absorption. More importantly, the NPs were also used for MRI. The relaxivity of the Ni-doped NPs was about 2.3 mM^{-1}S^{-1} which was nearly 8 times higher than that of PMAH-PEG-Ni^{2+}. In addition, the well-defined dual-modal nanoprobe was successfully used for in vivo lymph node PA and MR dual-modal imaging. We expected that this functional metal ions doping approach could be triggered to prepare other nanostructures, which would open up the possibility to engineer multifunctional nanosystem.

Acknowledgements

Notes and references

1   a) Y. L. Dai, H. H. Xiao, J. H. Liu, Q. H. Yuan, P. A. Ma , D. M. Yang, C. X. Li, Z. Y. Cheng, Z. Y. Hou, P. P. Yang and J. Lin, *J. Am. Chem. Soc.,* 2013, **135,** 18920; b) R. Chakravarty, H. F. Valdovinos, F. Chen , C. M. Lewis, P. A. Ellison, H. M. Luo, M. E. Meyerand, R. J. Nickles and W. B. Cai, *Adv. Mater.,* 2014, **26,** 5119; c) W. S. Guo, X. L. Sun, O. Jacobson, X. F. Yan, K. Min, A. Srivatsan, G. Niu, D. O. Kiesewetter, J. Chang and X. Y. Chen, *ACS Nano,* 2015, **9,** 488; d) D.Y. Gao, P. F. Zhang, Z. H. Sheng, D. H. Hu, P. Gong, C. Chen, Q. Wan, G. H. Gao and L. T. Cai, *Adv. Funct. Mater.,* 2014, **24,** 3897; e) L. Cheng, J. J. Liu, X. Gu, H. Gong, X. Z. Shi, T. Liu, C. Wang, X. Y. Wang, G.

Nanoscale Accepted Manuscript

COMMUNICATION **Journal Name**

Liu, H. Y. Xing, W. B. Bu, B. Q. Sun and Z. Liu, *Adv. Mater.,* 2014, **26,** 1886; f) Z. H. Sheng, L. Song, J. X. Zheng, D. H. Hu, M. He, M. B. Zheng, G. H. Gao, P. Gong, P. F. Zhang, Y. F. Ma and L. T. Cai, *Biomaterials,* 2013, **34,** 5236.

2 a) D. E. Lee, H. Koo, I. C. Sun, J. H. Ryu, K. Kim and I. C. Kwon, *Chem. Soc. Rev.*, 2012, **41,** 2656; b) K. Ding, L. H. Jing, C. Y. Liu, Y. Hou and M. Y. Gao, *Biomaterials*, 2014, **35,** 1608.

3 a) M. G. Harisinghani, J. Barentsz, P. F. Hahn, W. M. Deserno, S. Tabatabaei, C. H. van de Kaa, J. de la Rosette and R. Weissleder, *N. Engl. J. Med.,* 2003, **348,** 2491; b) L. R. Hirsch, R. J. Stafford, J. A. Bankson, S. R. Sershen, B. Rivera, R. E. Price, J. D. Hazle, N. J. Halas and J. L. West, *Proc. Natl. Acad. Sci.,* 2003, **100,** 13549.

4 a) L.V. Wang, *Nat. Photonics.,* 2009**, 3,** 503; b) S. H. Yang, D. Xing, Q. Zhou, L. Z. Xiang and Y. Q. Lao, *Med. Phys.,* 2007, **34,** 3294.

5 a) J. Yu , C. Yang, J. D. S. Li, Y. C. Ding, L. Zhang, M. Z. Yousaf, J. Lin, R. Pang, L. B. Wei, L. L. Xu, F. G. Sheng, C. H. Li, G. J. Li, L. Y. Zhao and Y. L. Hou, *Adv. Mater.,* 2014, **26,** 4114; b) M. F. Kircher, A. de la Zerda, J. V. Jokerst, C. L. Zavaleta, P. J. Kempen, E. Mittra, K. Pitter, R. Huang, C. Campos, F. Habte, R. Sinclair, C. W. Brennan, I. K. Mellinghoff, E. C. Holland and S. S. Gambhir, *Nat. Med.,* 2012, **15,** 829; c) K. Yang, L. Hu, X. Ma, S. Ye, L. Cheng, X. Shi, C. Li, Y. Li and Z. Liu, *Adv. Mater.,* 2012, **10,** 1868.

6 a) J. U. Menon, P. Jadeja, P. Tambe, K. Vu, B. Yuan and K. T. Nguyen, *Theranostics,* 2013, **3,** 152; b) O. Rabin, J. Manuel Perez, J. Grimm, G. Wojtkiewicz and R. Weissleder, *Nat. Mater.,* 2006, **5,** 118; c) M. P. Melancon, M. Zhou and C. Li, *Acc. Chem. Res.,* 2011, **44,** 947.

7 a) J. V. Jokerst, M. Thangaraj, P. J. Kempen, R. Sinclair and S. S. Gambhir, *ACS Nano,* 2012, **6,** 5920; b) W. Lu, Q. Huang, G. Ku, X. Wen, M. Zhou, D. Guzatov, P. Brecht, R. Su , A. Oraevsky, L. V. Wang and C. Li, *Biomaterials,* 2010, **31,** 2617; c) C. Kim, E. C. Cho, J. Chen, K. H. Song, L. Au, C. Favazza, Q. Zhang, C. M. Cobley, F. Gao, Y. N. Xia and L. V. Wang, *ACS Nano,* 2010, **4,** 4559.

8 a) W. Han, L. X. Yi, N. Zhao, A. W. Tang, M. Y. Gao and Z. Y. Tang, *J. Am. Chem. Soc.,* 2008, **130,** 13152; b) X. Liu, X. L. Wang, B. Zhou, W. Law, A. N. Cartwright and M. T. Swihart, *Adv. Funct. Mater.,* 2013, **23,** 1256; c) Q. W. Tian, M. H. Tang, Y. G. Sun, R. J. Zou, Z. G. Chen, M. F. Zhu, S. P. Yang, J. L. Wang, J. H. Wang and J. Q. Hu, *Adv. Mater.,* 2011, **23,** 3542; d) Q. W. Tian, F. R. Jiang, R. J. Zou, Q. Liu, Z. G. Chen, M. F. Zhu, S. P. Yang, J. L. Wang, J. H. Wang and J. Q. Hu, *ACS Nano,* 2011, **5,** 9761; e) C. M. Hessel, V. P. Pattani, M. Rasch, M. G. Panthani, B. Koo, J. W. Tunnell and B. A. Korgel, *Nano Lett.,* 2011, **11,** 2560; f) A. C. Poulose, S. Veeranarayanan, M. S. Mohamed, Y. Sakamoto, N. Hirosawa, Y. Suzuki, M. Zhang, M. Yudasaka, N. Radhakrishnan, T. Maekawa, P. V. Mohanan and D. S. Kumar, *Nanoscale,*2015,**7,**13061.

9 X. Liu, W. C. Law, M. Jeon, X. Wang, M. Liu, C. Kim, P. N. Prasad and M. T. Swihart, *Adv. Health. Mater.,* 2013, **2,** 952.

10 a) H. Y. Xing, S. J. Zhang, W. B. Bu, X.P. Zheng, L. J. Wang, Q. F. Xiao, D. L. Ni, J. M. Zhang, L. P. Zhou, W. J. Peng, K. L. Zhao, Y. Q. Hua and J. L. Shi, *Adv. Mater.,* 2014, **26,** 3867; b) W. Tang, Z. P. Zhen, C. Yang, L. N. Wang, T. Cowger, H. M. Chen, T. Todd, K. Hekmatyar, Q. Zhao, Y. L. Hou and J. Xie, *Small,* 2014, **10,** 1245; c) X. R. Song, X. Y. Wang, S. X. Yu, J. B. Cao, S. H. Li, J. Li, G. Liu, H. H. Yang and X. Y. Chen, *Adv. Mater.,* 2015, **27,** 3285.

11 a) T. Zhou, B. Y. Wu and D. Xing, *J. Mater. Chem.,* 2012, **22,** 470; b) X. G. Ding, C. H. Liow, M. X. Zhang, R. J. Huang, C. Y. Li, H. Shen, M. Y. Liu, Y. Zou, N. Gao, Z. J. Zhang, Y. G. Li, Q. B. Wang, S. Z. Li and J. Jiang, *J. Am. Chem. Soc.,* 2014, **136,** 15684; c) C. Liang, X. J. Song, Q. Chen, T. Liu, G. S. Song , R. Peng and Z. Liu, *small,* DOI: DOI: 10.1002/smll.201501197; d) Q. W. Tian, J. Q. Hu, Y. H. Zhu, R. J. Zou, Z. G. Chen, S. P.

Yang, R. W. Li, Q. Q. Su, Y. Han and X. G. Liu, *J. Am. Chem. Soc.,* 2013, **135,** 8571; e) Y. D. Jin, C. X. Jia, S. W. Huang, M. O'Donnell and X. H. Gao, *Nat.Commun.,*2010, **1,** 1; f) H. Qin, T. Zhou, S. H. Yang, Q. Chen and D. Xing, *Nanomedicine,* 2013, **8,** 1611.

12 a) W. R. Sanhai, J. H. Sakamoto, R. Canady and M. Ferrari, *Nat. Nanotechnol.,* 2008, **3,** 242.

13 M. Zhou, R. Zhang, M. Huang, W. Lu, S. L. Song, M. P. Melancon, M. Tian, D. Liang and C. Li, *J. Am. Chem. Soc.,* 2010, **132,** 15351.

14 a) X. Liu, X. L. Wang and M. T. Swihart, *Chem. Mater.*, 2013, **25,** 4402; b) J. M. Luther, P. K. Jain, T. Ewers and A. P. Alivisatos, *Nat. Mater.,* 2011, **10,** 361; c) Y. X. Zhao, H. C. Pan, Y. B. Lou , X. F. Qiu, J. J. Zhu and C. Burda, *J. Am. Chem. Soc.,* 2009, **131,** 4253; d) H. H. Ye, A. W. Tang, C. H. Yang, K. Li, Y. B. Hou and F. Teng, *CrystEngComm.,* 2014, **16,** 8684.

15 a) I. Kriegel, C. Y. Jiang, J. Rodríguez-Fernández, R. D. Schaller, D. V. Talapin, E. D. Como and J. Feldmann, *J. Am. Chem. Soc.*, 2012, **134,** 1583; b) X. Liu, X. L. Wang and M. T. Swihart, *Chem. Mater.,* 2013, **25,** 4402.

16 a) M. B. Sigman, Jr., A. Ghezelbash, T. Hanrath, A. E. Saunders, F. Lee and B. A. Korgel, *J. Am. Chem. Soc.,* 2003, **125,** 16050; (b) A. Ghezelbash, M. B. Sigman, Jr. and B. A. Korgel, *Nano Lett.,* 2004, **4,** 537; (c) A. Ghezelbash and B. A. Korgel, *Langmuir,* 2005, **21,** 9451.

17 a) P. F. Zhang, S. H. Liu, D. Y. Gao, D. H. Hu, P. Gong, Z. H. Sheng, J. Z. Deng, Y. F. Ma and L. T. Cai, *J. Am. Chem. Soc.,* 2012, **20,** 8388; b) D. H. Hu, P. F. Zhang, P. Gong, S. H. Lian, D. Y. Gao and L. T. Cai, *Nanoscale,* 2011, **3,** 4724.

18 a) J. S. Ananta, B. Godin, R. Sethi, L. Moriggi, X. W. Liu, R. E. Serda, R. Krishnamurthy, R. Muthupillai, R. D. Bolskar, L. Helm, M. Ferrari, L. J. Wilson and P. Decuzzi, *Nat. Nanotechnol.,* 2010, **5,** 815; b) A. Gizzatov, J. Key, S. Aryal, J. Ananta, A. Cervadoro, A. L. Palange, M. Fasano, C. Stigliano, M. Zhong, D. D. Mascolo, A. Guven, E. Chiavazzo, P. Asinari, X.W. Liu, M. Ferrari, L. J. Wilson and P. Decuzzi, *Adv. Funct. Mater.,* 2014, **24,** 4584; c) X. L. Hu, G. H. Liu, Y. Li, X. R. Wang, and S. Y. Liu, *J. Am. Chem. Soc.* 2015, **137,** 362.

19 M. P. B. Rohrer, H. Bauer, J. Mintorovitch, M. Requardt and H. J. Weinmann, *Invest. Radiol.,* 2005, **40,** 715.

20 P. N. Prasad, *Introduction to Nanomedicine and Nanobioengineering,* John Wiley & Sons, Hoboken, New Jersey **2012**.